# Observation of Massless and Massive Collective Excitations with Faraday Patterns in a Two-Component Superfluid

R. Cominotti, A. Berti, A. Farolfi, A. Zenesini,* G. Lamporesi,† I. Carusotto, A. Recati,‡ and G. Ferrari
*INO-CNR BEC Center and Dipartimento di Fisica, Università di Trento, and Trento Institute for Fundamental Physics and Applications, INFN, 38123 Povo, Italy*

(Received 17 December 2021; revised 28 January 2022; accepted 19 April 2022; published 23 May 2022)

We report on the experimental measurement of the dispersion relation of the density and spin collective excitation modes in an elongated two-component superfluid of ultracold bosonic atoms. Our parametric spectroscopic technique is based on the external modulation of the transverse confinement frequency, leading to the formation of density and spin Faraday waves. We show that the application of a coherent coupling between the two components reduces the phase symmetry and gives a finite mass to the spin modes.

DOI: 10.1103/PhysRevLett.128.210401

The concept of collective excitations is a cornerstone for our understanding of the physics of condensed matter systems. In particular, arguments based on their dispersion relation have provided first insight on the microscopic origin of superfluidity in liquid helium [1]. In the specific case of dilute atomic Bose-Einstein condensates (BEC), the Bogoliubov theory, based on a linearized quantum theory around a condensate, provides quantitative predictions for the dispersion relation, with a gapless (massless) sonic behavior at small wave vectors followed by a quadratic single-particle one at larger wave vectors [2].

The situation gets more interesting in the case of two-component superfluids, whose collective excitation spectrum consists of two gapless branches for the spontaneously broken $\mathrm{U}(1)\times\mathrm{U}(1)$ symmetry due to the conservation of particle number in each component. For equal masses and interaction constants of the two components, the two branches are associated with oscillations of the total density or of the density difference, the so-called "density" and "spin" modes [3]. At low $k$, both branches have a linear dispersion, yet with generally distinct values of the speed of sound. If the particle number in each component is not conserved, e.g., by applying a field that coherently couples the two components, exciting the condensate relative phase requires an energy cost. As a result, while the massless nature of the total density mode is protected by the Goldstone theorem associated with the remaining U(1) symmetry, the spin mode acquires a finite mass [4].

Precise information on the Bogoliubov dispersion of single-component condensates was extracted using Bragg spectroscopy [5]. Parametric excitation of a superfluid was pioneered using a time-dependent modulation of the optical lattice depth [6–9], by acting on the transverse potential of an elongated harmonically trapped BEC [10–12] or through a modulation of the interaction constant [13–15]. Distinct spin and density sound velocities were measured in a two-component sodium system by locally perturbing the system with spin sensitive or insensitive potential [16]. Two-dimensional bosonic superfluids [17] and strongly interacting superfluids [18,19] were also recently investigated.

In this Letter, we apply the parametric excitation technique to the novel case of a two-component BEC of ultracold sodium atoms in two spin states. A well-controlled generation of Faraday waves in both the density and in the spin channel allows us to perform a first quantitative and complete measurement of the dispersion relation of the two branches of collective density and spin excitations.

In an intuitive way, one can understand the parametric excitation process as the emission of a pair of phonons (of frequency $\omega_M/2$ and opposite wave vectors $\pm k$) by some classical external drive at $\omega_M$, as sketched in Fig. 1. The two modes lead to a spatial pattern oscillating in time, known as a Faraday wave [see Fig. 2(b)]. Its spatial periodicity is $2\pi/k$ and its visibility oscillates in time at $\omega_M$ (see, e.g., [20]).

As pictorially shown in Fig. 1, the parametric process is active on both density and spin channels (hereafter labeled as $d$ and $s$). In particular, energy-momentum conservation predicts different values for the wave vector $k$ of the emitted density and spin excitations. Concretely, for a coherently coupled BEC of atoms with mass $m$, the dispersion relations read (see Ref. [3] and references therein) as follows:

$$\omega_d(k)=\sqrt{\frac{\hbar k^2}{2m}\left(\frac{\hbar k^2}{2m}+\frac{2\mu_d}{\hbar}\right)} \tag{1}$$

$$\omega_s(k)=\sqrt{\left(\frac{\hbar k^2}{2m}+\Omega_R\right)\left(\frac{\hbar k^2}{2m}+\frac{2\mu_s}{\hbar}+\Omega_R\right)}. \tag{2}$$

 

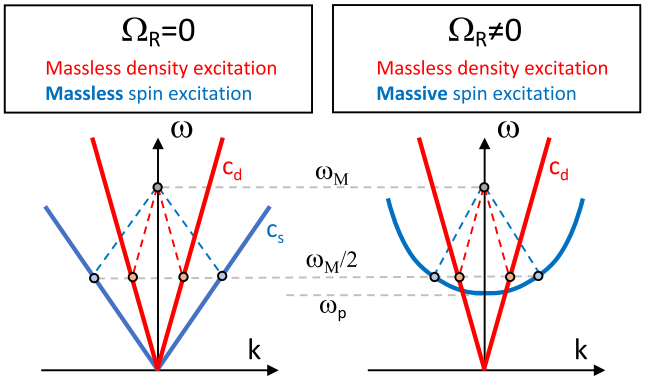


FIG. 1. Generation mechanism of excitation pairs in the density and spin branches of a two-component system. The external excitation at $\omega_M$ is converted into two excitations with opposite wave vectors and half the energy. In the absence of coupling between the two components, $\Omega_R = 0$ (left), two symmetries are preserved and both modes have a linear behavior, with density speed of sound $c_d$ and spin speed of sound $c_s$. When a coherent coupling is present, $\Omega_R \neq 0$ (right), one of the two symmetries is broken, introducing a curvature in the spin dispersion relation, which makes the excitation acquire a mass.

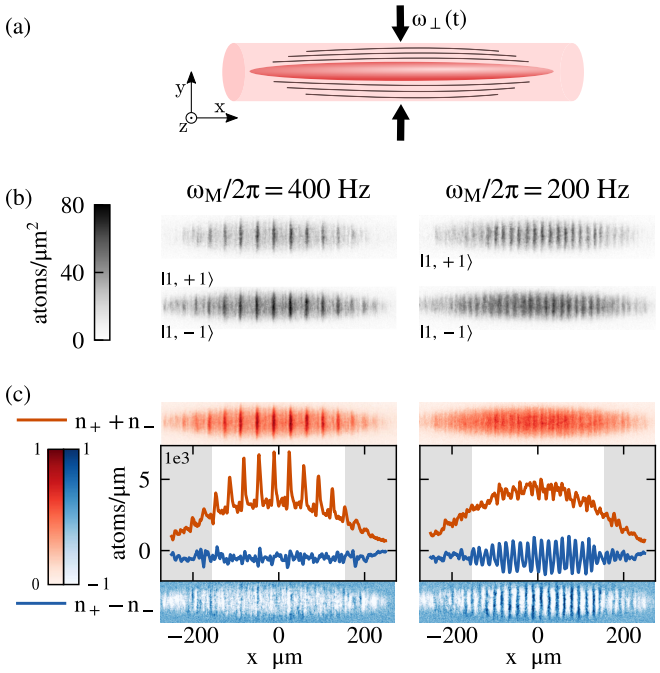


FIG. 2. Density and spin Faraday patterns. (a) Sketch of the experimental configuration. The transverse trapping frequency is modulated in time at frequency $\omega_M$, periodically compressing the elongated condensate. (b) The parametrically generated excitations appear as a spatial pattern with a well-defined wavelength along the axis of the condensate. (c) Density (red) and spin (blue) 2D experimental patterns and corresponding integrated 1D profiles for $\omega_M/2\pi = 400$ Hz (left) and $\omega_M/2\pi = 200$ Hz (right).

Here, $\mu_{d,s} = (g \pm g_{12})n_{\mathrm{eff},d,s}/2$ are the effective chemical potentials for the density and spin channels, where $g$ and $g_{12}$ are the intra- and intercomponent interaction constants, and $n_{\mathrm{eff},d} = n_0/2$ and $n_{\mathrm{eff},s} = 2n_0/3$, the effective densities after properly including the effects of the geometrical reduction [21]. The strength of the coherent coupling, which breaks the relative atom number conservation, is given by the Rabi frequency $\Omega_R$. For small $k$ and $\Omega_R = 0$, both channels, Eqs. (1) and (2), show the soniclike behavior $\omega_{d,s}(k) \simeq c_{d,s}|k|$ with speeds of sound $c_{d,s} = \sqrt{\mu_{d,s}/m}$.

The coherent coupling $\Omega_R$ has no effect on the density branch, while a frequency gap $\omega_p = \sqrt{\Omega_R(\Omega_R + 2\mu_s/\hbar)}$ opens in the spin branch, which then turns massive, $\omega_s(k) \simeq \omega_p + \hbar k^2/(2M)$, with an effective mass $M = 2m\omega_p\Omega_R/(\omega_p^2 + \Omega_R^2)$. As already mentioned, the presence of a gap at $k = 0$ in the spin channel originates from the explicit breaking of the continuous symmetry U(1), related to the conservation of the relative particle number. For noninteracting atoms the gap is simply $\Omega_R$ and corresponds to the energy cost to slightly move the ground state from its position, i.e., the cost to modify the relative phase of the two hyperfine wave functions locked by an external drive. In the presence of many-body interactions, the problems becomes equivalent to the so-called internal Josephson effect [24,25] and $\omega_p$ corresponds to the frequency of small oscillations around the homogeneous ground state, which for this reason is also called plasma frequency (see the recent review Ref. [26] and reference therein).

We start our experiments by preparing a BEC of $10^6$ $^{23}$Na atoms in the $|F, m_F\rangle = |1, -1\rangle$ internal state, $F$ being the total atomic angular momentum and $m_F$ its projection on the quantization axis, set by a uniform magnetic field [27]. The BEC (with negligible thermal component) is held in a cylindrically symmetric single-beam optical trap with trapping frequencies $\omega_\perp/2\pi = 1$ kHz and $\omega_x/2\pi = 10$ Hz, leading to a Thomas-Fermi profile with radii $r_\perp = 3$ $\mu$m and $r_x = 300$ $\mu$m for the transverse and longitudinal directions, respectively.

The two-component BEC is then prepared through an adiabatic rapid passage sequence [28,29], which coherently transfers half of the atomic population to the $|1, 1\rangle$ state, using a two-photon microwave transition [21]. At the end of the adiabatic rapid passage, the microwave drive is either completely switched off (experiments in Figs. 2 and 3) or kept on at the desired value of the coherent coupling between the two components (experiments in Fig. 4).

As done in Ref. [10], we induce Faraday waves by modulating the transverse trapping frequency as $\omega_\perp(t) = \omega_\perp(0)[1 + \alpha \sin(\omega_M t)]$, with frequency $\omega_M$ and amplitude $\alpha \in [0.38\text{–}0.6]$ [Fig. 2(a)]. The modulation is applied for a time $t \in [50\text{–}400]$ ms. Since $\omega_x \ll \omega_M < \omega_\perp(t)$, the transverse size adiabatically changes in time following the periodic compression and decompression of the potential. In this way no transverse excitation is generated. Conversely, axial modes can be excited, leading to

longitudinal (1D) Faraday waves [20,30]. At the end of the modulation, the trapping potential is suddenly removed and the atoms in the $|1,-1\rangle$ ($|1,+1\rangle$) state are selectively imaged after a short time of flight of 2 ms (3 ms) [Fig. 2(b)]. Because of the short duration of the time of flight stage, our very elongated condensate expands only in the transverse directions, leaving the axial distribution practically unchanged. We can therefore integrate the absorption images displayed in Fig. 2(b) over the transverse directions to extract the 1D densities $n_\pm$ in the $|1,\pm1\rangle$ spin states and, from these, the total density $(n_+ + n_-)$ and spin $(n_+ - n_-)$ profiles along $x$. In Fig. 2(c), we present typical profiles in the absence of coherent coupling for two different values of the modulation frequency. Depending on the modulation frequency, we observe that a periodic pattern can be formed in the density (left) or in the spin (right) profiles.

The strength and periodicity of the spatial modulations can be quantified by calculating the power spectral density (PSD) of the 1D profiles as follows:

$$\mathrm{PSD}_{d,s}(k) = \left| \int (n_+ \pm n_-) e^{ikx} dx \right|^2. \tag{3}$$

To suppress inhomogeneous broadening effects, we restrict the analysis to the central 300 $\mu$m of the condensate [white region in Fig. 2(c)].

Examples of the time evolution of the PSD are shown in the insets of Figs. 3(a) and 3(b). The PSD displays periodic oscillations at specific values of $k$, with the same frequency of the modulation. This behavior is typical of Faraday waves and in close agreement with the theoretical predictions for a single-component condensate [20,30]: the visibility of both spin and density excitations is maximal in time when $\omega_\perp(t)$ is minimum [$t = (2n + 3/2)\pi/\omega_M$ with $n \in \mathbb{Z}$]. Being spin and density excitations always in phase, the ratio between the two visibilities remains constant within a modulation period. While the position of the PSD peak is stable, its absolute height is strongly dependent on the chosen values of the modulation strength and duration. In order to optimize the visibility of the features for all the modulation frequencies, the duration or amplitude of the modulation is empirically optimized and the atoms are released always at times corresponding to a minimum in $\omega_\perp(t)$ (see insets in Fig. 3). This protocol allows us to obtain the PSD as a function of the modulation frequency $\omega_M$ and the wave vector $k$ of the induced pattern reported as color plots in Figs. 3 and 4.

The values of $k$ for which the pattern is strongest follow extremely well the theoretically predicted dispersion relations [Eqs. (1) and (2)] with $\Omega_R = 0$, as reported in Fig. 3. Here, the only nontrivial parameter is the BEC peak density $n_0$ of the 3D distribution, which is independently calibrated by measuring the plasma frequency of the two-component BEC at the center of the cloud [21,29],

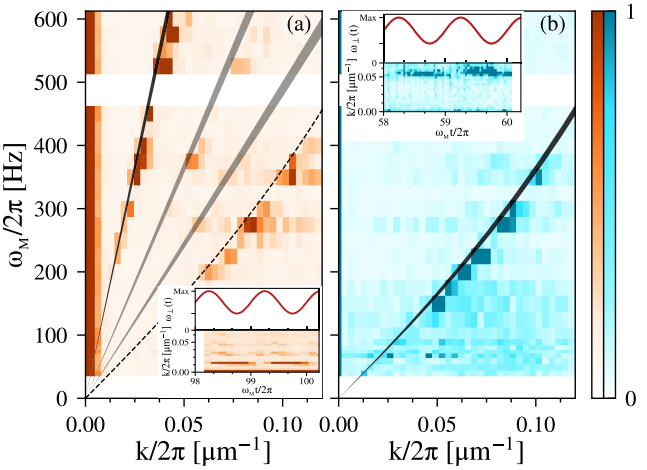


FIG. 3. PSD of density (a) and spin (b) excitations as a function of the modulation frequency. The thick lines indicate theoretical predictions [Eqs. (1) and (2)] for the dispersion relations (dark) and subharmonics (light) (see text), with $\Omega_R = 0$ and no fitting parameters. The line thickness corresponds to one standard deviation confidence interval originating from the uncertainty in the atomic density. Insets show the modulation amplitude in time and the corresponding fringe visibility for $\omega_M/2\pi = 200$ Hz. The dashed line in panel (a) indicates the position of the spin branch, where a spurious signal is present due to the crosstalk between spin and density modes.

leading to the estimated chemical potentials $\mu_d/h = 3$ kHz and $\mu_s/h = 145$ Hz.

In the density channel, the $k$ position of the peak depends linearly on the modulation frequency as $k \simeq \omega_M/(2c_d)$, since all the probed frequencies are well in the sonic region of the dispersion relation $\omega_M \ll \mu_d/\hbar$. In contrast, in the spin channel the linear dependence $k \simeq \omega_M/(2c_s)$ is restricted to modulation frequencies $\omega_M \lesssim 2\mu_s/\hbar$, whereas for larger $\omega_M$, a deviation from the linear behavior is observed, in agreement with the supersonic nature of the Bogoliubov dispersion.

We notice that a residual signature of the spin modes is visible on the density spectra and vice versa [see dashed lines in Figs. 3(a) and 4(b)] This originates from a weak coupling between the spin and density modes due to slight imbalance of the density in the two spin states, as well as from some crosstalk between the two spin components in the imaging technique [29].

We turn now to the analogous measurement performed in the presence of the coherent coupling $\Omega_R \neq 0$, shown in Fig. 4. In order to observe collective behaviors in the spin channel, we need to have $\hbar\Omega_R < 2\mu_s$, a condition that ensures also that the adiabaticity condition is fulfilled, having $\omega_p \ll \omega_\perp$. Operating in this regime is experimentally possible thanks to the $\mu G$-level stability in the magnetic field that is provided by the magnetic shielding surrounding our setup [21,31]. This magnetic field stability corresponds to a frequency stability of the atomic resonance at the level of a few Hz.

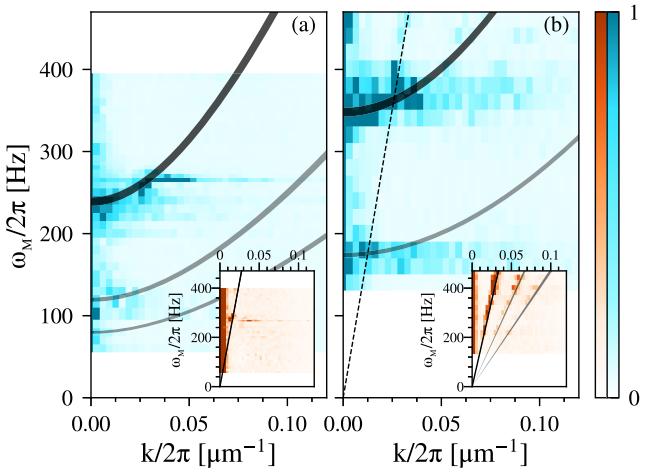


FIG. 4. PSD of the spin excitations in the presence of a coherent coupling. In (a), $\omega_p/2\pi = 120$ Hz, $\Omega_R/2\pi = 33$ Hz, and $\mu_s/h = 225$ Hz; in (b), $\omega_p/2\pi = 175$ Hz, $\Omega_R/2\pi = 80$ Hz, and $\mu_s/h = 150$ Hz. The thick lines indicate the theoretical predictions [Eqs. (1) and (2)] for the dispersion relations (dark) and subharmonics (light) (see text). The line thickness corresponds to one standard deviation confidence interval originating from the uncertainty in the atomic density. Insets show the corresponding PSD of the density channel (unaffected by the coupling). The dashed line in panel (b) indicates the position of the density branch, where a spurious signal is present due to the crosstalk between spin and density modes.

The results for $\Omega_R \neq 0$ are discussed in the following, with peculiar attention to (i) the *massive dispersion* in the spin channel; (ii) the *sonic dispersion* in the density channel, unaffected by the coherent coupling; and (iii) the *scaling* of the gap with $\omega_p$.

We verified, both numerically and experimentally, that the formation of the spin pattern occurs on much faster timescales, as compared to the case $\Omega_R = 0$, when the modulation frequency $\omega_M$ is close to $2\omega_p$. Therefore, in order to access all the above mentioned points, different values of the amplitude and modulation time were used for the datasets shown in Figs. 4(a) and 4(b).

To address point (i), we use a short modulation time that allows one to obtain a clean signal in the spin channel around $\omega_M \simeq 2\omega_p$, showing the massive character of spin collective excitations [Fig. 4(a)]. This choice inhibits the observation of the dispersion relation in the density channel (see the inset). To overcome such a difficulty, we increase depth and duration of the periodic driving and the corresponding measurement is shown in Fig. 4(b): the inset reveals how the excited wave vector $k$ still depends linearly on $\omega_M$, regardless of the coherent coupling [point (ii)]. Unfortunately, at such long modulation times, spin modes around the plasma frequency are excited strongly in the nonperturbative regime, which results in the broadening of the spectrum in $k$ space: hence, the blue horizontal stripes in Fig. 4(b) should not be confused with the expected dispersion relation Eq. (2).

For what concerns point (iii), the different values of $\Omega_R/2\pi = 33$ Hz and $\Omega_R/2\pi = 80$ Hz in the datasets of panels (a) and (b) of Fig. 4 illustrate the scaling of the gap size with $\omega_p$. In the spin channel an appreciable signal is only visible above $2\omega_p$. Above this point, the $k$ position of the peak remains in very good agreement with the expected massive dispersion relation of the spin excitations (continuous black line). For the data in Figs. 4(a) and 4(b), the effective mass is about 25% and 75% of the atomic mass, respectively.

While the dispersion relations [Eqs. (1) and (2)] are consistent with the dominant signal in the PSD of Figs. 3 and 4, the additional signals at subharmonic frequencies (gray lines) are typical of Faraday instabilities described in terms of the Mathieu equation [21], which is known to show instability (resonance) regions around $\omega_M = 2\omega(k)/l$, with $l$ a positive integer number [32]. We verified that such signals are not originated by residual anharmonicities of the optical trap modulation.

In conclusion, in this Letter we have made use of a parametric excitation technique to perform a detailed measurement of the dispersion relation of the longitudinal density and spin collective excitations of an elongated two-component BEC. The accuracy and flexibility of our spectroscopic technique directly hint at its application to more complex phenomena in quantum mixtures. Specifically, in the case of an interspecies interaction larger than the intraspecies one, we could study spin excitations when crossing the ferromagnetic phase (see Ref. [3] and reference therein). Another relevant application of our technique would be the study of the dispersion relations in the various phases of spin-orbit coupled mixtures. Particularly interesting is the rotonization of the spectrum and the appearance of a new Goldstone mode in the so-called stripe phase (see Ref. [33] and reference therein).

It is also worth mentioning that the parametric excitation of the spin modes in our system is essentially equivalent to the so-called parallel pumping amplification, which has been taking on a very important role in magnonics [34]. In this respect, a byproduct of the present work is to provide further evidence that our platform, as already shown in [35], provides new insights in the dynamics of magnetic materials.

From a yet different perspective, analog models [36] based on two-component atomic BECs are a promising platform for quantitative studies of quantum field theories on curved space-times, such as cosmological particle creation and analog Hawking radiation [37–40]. In particular, the control on the mass of the spin excitations, which was demonstrated here via coherent coupling, is of great interest in view of extending this research to the case of massive fields interacting with the gravitational background. On a longer run, the complex dynamics obtained when the externally imposed modulation of the trap parameters is replaced with an excitation of the transverse

degrees of freedom of the BEC may provide information on backreaction phenomena of the quantum field theory on the background space-time [41].

We thank F. Dalfovo and S. Stringari for fruitful discussions and for their critical reading of the manuscript. I. C. acknowledges continuous collaboration with S. G. Butera. We acknowledge funding from Provincia Autonoma di Trento, from INFN through the FISH project and from the Italian MIUR under the PRIN2017 project CEnTraL (Protocol No. 20172H2SC4). This work was supported by Q@TN, the joint lab between University of Trento, FBK—Fondazione Bruno Kessler, INFN—National Institute for Nuclear Physics and CNR—National Research Council.

R. C. and A. B. contributed equally to this work.

*Corresponding author.
alessandro.zenesini@ino.cnr.it
†Corresponding author.
giacomo.lamporesi@ino.cnr.it
‡Corresponding author.
alessio.recati@ino.cnr.it

[1] D. Pines and P. Nozieres, *The Theory of Quantum Liquids* (W. A. Benjamin, New York, 1996), Vol. 1.
[2] L. Pitaevskii and S. Stringari, *Bose-Einstein Condensation and Superfluidity*, International Series of Monographs on Physics (Oxford University Press, Oxford, 2016).
[3] M. Abad and A. Recati, A study of coherently coupled two-component Bose-Einstein condensates, Eur. Phys. J. D **67**, 148 (2013).
[4] E. V. Goldstein and P. Meystre, Quasiparticle instabilities in multicomponent atomic condensates, Phys. Rev. A **55**, 2935 (1997).
[5] J. Steinhauer, R. Ozeri, N. Katz, and N. Davidson, Excitation Spectrum of a Bose-Einstein Condensate, Phys. Rev. Lett. **88**, 120407 (2002).
[6] C. Schori, T. Stöferle, H. Moritz, M. Köhl, and T. Esslinger, Excitations of a Superfluid in a Three-Dimensional Optical Lattice, Phys. Rev. Lett. **93**, 240402 (2004).
[7] T. Stöferle, H. Moritz, C. Schori, M. Köhl, and T. Esslinger, Transition from a Strongly Interacting 1D Superfluid to a Mott Insulator, Phys. Rev. Lett. **92**, 130403 (2004).
[8] M. Krämer, C. Tozzo, and F. Dalfovo, Parametric excitation of a Bose-Einstein condensate in a one-dimensional optical lattice, Phys. Rev. A **71**, 061602(R) (2005).
[9] C. Tozzo, M. Krämer, and F. Dalfovo, Stability diagram and growth rate of parametric resonances in Bose-Einstein condensates in one-dimensional optical lattices, Phys. Rev. A **72**, 023613 (2005).
[10] P. Engels, C. Atherton, and M. A. Hoefer, Observation of Faraday Waves in a Bose-Einstein Condensate, Phys. Rev. Lett. **98**, 095301 (2007).
[11] J.-C. Jaskula, G. B. Partridge, M. Bonneau, R. Lopes, J. Ruaudel, D. Boiron, and C. I. Westbrook, Acoustic Analog to the Dynamical Casimir Effect in a Bose-Einstein Condensate, Phys. Rev. Lett. **109**, 220401 (2012).
[12] J. Smits, L. Liao, H. T. C. Stoof, and P. van der Straten, Observation of a Space-Time Crystal in a Superfluid Quantum Gas, Phys. Rev. Lett. **121**, 185301 (2018).
[13] S. E. Pollack, D. Dries, R. G. Hulet, K. M. F. Magalhães, E. A. L. Henn, E. R. F. Ramos, M. A. Caracanhas, and V. S. Bagnato, Collective excitation of a Bose-Einstein condensate by modulation of the atomic scattering length, Phys. Rev. A **81**, 053627 (2010).
[14] C.-L. Hung, V. Gurarie, and C. Chin, From cosmology to cold atoms: Observation of Sakharov oscillations in a quenched atomic superfluid, Science **341**, 1213 (2013).
[15] J. H. V. Nguyen, M. C. Tsatsos, D. Luo, A. U. J. Lode, G. D. Telles, V. S. Bagnato, and R. G. Hulet, Parametric Excitation of a Bose-Einstein Condensate: From Faraday Waves to Granulation, Phys. Rev. X **9**, 011052 (2019).
[16] J. H. Kim, D. Hong, and Y. Shin, Observation of two sound modes in a binary superfluid gas, Phys. Rev. A **101**, 061601 (R) (2020).
[17] Z. Zhang, K.-X. Yao, L. Feng, J. Hu, and C. Chin, Pattern formation in a driven Bose-Einstein condensate, Nat. Phys. **16**, 652 (2020).
[18] P. B. Patel, Z. Yan, B. Mukherjee, R. J. Fletcher, J. Struck, and M. W. Zwierlein, Universal sound diffusion in a strongly interacting Fermi gas, Science **370**, 1222 (2020).
[19] D. Hernández-Rajkov, J. E. Padilla-Castillo, A. del Río-Lima, A. Gutiérrez-Valdés, F. J. Poveda-Cuevas, and J. A. Seman, Faraday waves in strongly interacting superfluids, New J. Phys. **23**, 103038 (2021).
[20] A. I. Nicolin, R. Carretero-González, and P. G. Kevrekidis, Faraday waves in Bose-Einstein condensates, Phys. Rev. A **76**, 063609 (2007).
[21] See Supplemental Material at http://link.aps.org/supplemental/10.1103/PhysRevLett.128.210401 for additional information on experimental calibrations and theoretical models, which includes Refs. [22,23].
[22] T. Bienaimé, E. Fava, G. Colzi, C. Mordini, S. Serafini, C. Qu, S. Stringari, G. Lamporesi, and G. Ferrari, Spin-dipole oscillation and polarizability of a binary Bose-Einstein condensate near the miscible-immiscible phase transition, Phys. Rev. A **94**, 063652 (2016).
[23] M. Bukov and M. Heyl, Parametric instability in periodically driven Luttinger liquids, Phys. Rev. B **86**, 054304 (2012).
[24] J. Williams, R. Walser, J. Cooper, E. Cornell, and M. Holland, Nonlinear Josephson-type oscillations of a driven, two-component Bose-Einstein condensate, Phys. Rev. A **59**, R31 (1999).
[25] T. Zibold, E. Nicklas, C. Gross, and M. K. Oberthaler, Classical Bifurcation at the Transition from Rabi to Josephson Dynamics, Phys. Rev. Lett. **105**, 204101 (2010).
[26] A. Recati and S. Stringari, Coherently coupled mixtures of ultracold atomic gases, Annu. Rev. Condens. Matter Phys. **13**, 407 (2022).
[27] G. Colzi, E. Fava, M. Barbiero, C. Mordini, G. Lamporesi, and G. Ferrari, Production of large Bose-Einstein condensates in a magnetic-shield-compatible hybrid trap, Phys. Rev. A **97**, 053625 (2018).
[28] A. Farolfi, D. Trypogeorgos, C. Mordini, G. Lamporesi, and G. Ferrari, Observation of Magnetic Solitons in

Two-Component Bose-Einstein Condensates, Phys. Rev. Lett. **125**, 030401 (2020).
[29] A. Farolfi, A. Zenesini, R. Cominotti, D. Trypogeorgos, A. Recati, G. Lamporesi, and G. Ferrari, Manipulation of an elongated internal Josephson junction of bosonic atoms, Phys. Rev. A **104**, 023326 (2021).
[30] M. Modugno, C. Tozzo, and F. Dalfovo, Detecting phonons and persistent currents in toroidal Bose-Einstein condensates by means of pattern formation, Phys. Rev. A **74**, 061601(R) (2006).
[31] A. Farolfi, D. Trypogeorgos, G. Colzi, E. Fava, G. Lamporesi, and G. Ferrari, Design and characterization of a compact magnetic shield for ultracold atomic gas experiments, Rev. Sci. Instrum. **90**, 115114 (2019).
[32] L. Landau and E. Lifshitz, On the theory of the dispersion of magnetic permeability in ferromagnetic bodies, Phys. Z. Sowjetunion **8**, 153 (1935).
[33] Y. Li, G. I. Martone, and S. Stringari, Spin-orbit-coupled Bose-Einstein condensates, in *Annual Review of Cold Atoms and Molecules* (World Scientific, 2015), Chap. 5, pp. 201–250.
[34] T. Brächer, P. Pirro, and B. Hillebrands, Parallel pumping for magnon spintronics: Amplification and manipulation of magnon spin currents on the micron-scale, Phys. Rep. **699**, 1 (2017).
[35] A. Farolfi, A. Zenesini, D. Trypogeorgos, C. Mordini, A. Gallemí, A. Roy, A. Recati, G. Lamporesi, and G. Ferrari, Quantum-torque-induced breaking of magnetic interfaces in ultracold gases, Nat. Phys. **17**, 1359 (2021).
[36] C. Barceló, S. Liberati, and M. Visser, Analogue gravity, Living Rev. Relativity **14**, 3 (2011).
[37] U. R. Fischer and R. Schützhold, Quantum simulation of cosmic inflation in two-component Bose-Einstein condensates, Phys. Rev. A **70**, 063615 (2004).
[38] M. Visser and S. Weinfurtner, Massive Klein-Gordon equation from a Bose-Einstein-condensation-based analogue spacetime, Phys. Rev. D **72**, 044020 (2005).
[39] S. Butera and I. Carusotto, Particle creation in the spin modes of a dynamically oscillating two-component Bose-Einstein condensate, Phys. Rev. D **104**, 083503 (2021).
[40] S. Butera, P. Öhberg, and I. Carusotto, Black-hole lasing in coherently coupled two-component atomic condensates, Phys. Rev. A **96**, 013611 (2017).
[41] S. Butera and I. Carusotto (to be published).